

Charge regulation radically modifies electrostatics in membrane stacks

Arghya Majee^{1,2,*}, Markus Bier^{1,2,3}, Ralf Blossey⁴, and Rudolf Podgornik^{5,6}

¹*Max-Planck-Institut für Intelligente Systeme,
Heisenbergstr. 3, 70569 Stuttgart, Germany*

²*IV. Institut für Theoretische Physik,
Universität Stuttgart, Pfaffenwaldring 57,
70569 Stuttgart, Germany*

³*Fakultät Angewandte Natur- und Geisteswissenschaften,
Hochschule für Angewandte Wissenschaften Würzburg-Schweinfurt,
Ignaz-Schön-Str. 11, 97421 Schweinfurt, Germany*

⁴*Université de Lille, CNRS,
UMR8576 Unité de Glycobiologie Structurale et Fonctionnelle (UGSF),
F-59000 Lille, France*

⁵*School of Physical Sciences and Kavli Institute for Theoretical Sciences,
University of Chinese Academy of Sciences,
Beijing 100049, China*

⁶*CAS Key Laboratory of Soft Matter Physics,
Institute of Physics, Chinese Academy of Sciences,
Beijing 100190, China*

(Dated: November 6, 2019)

Abstract

Motivated by biological membrane-containing organelles in plants and photosynthetic bacteria, we study charge regulation in a model membrane stack. Considering (de)protonation as the simplest mechanism of charge equilibration between the membranes and with the bathing environment, we uncover a symmetry-broken charge state in the stack with a quasiperiodic effective charge sequence. In the case of a monovalent bathing salt solution our model predicts complex, inhomogeneous charge equilibria depending on the strength of the (de)protonation reaction, salt concentration, intermembrane separation, and their number in the stack. Our results shed light on the basic reorganization mechanism of thylakoid membrane stacks.

* majee@is.mpg.de

I. INTRODUCTION

The charge regulation mechanism, described originally in the 1920's [1] and later developed by Kirkwood and Schumaker [2], Marcus [3] and Lifson [4] has become a topic of considerable research interest in recent years [5–9]. Charge regulation refers to the situation in which the local charge on a solvated surface responds to changes in the environment, such as local pH, dielectric inhomogeneities, salt concentrations, etc. The presence of dissociable groups, in particular on biological surfaces, then allows the surface charge to adapt to local and global solution conditions. As a consequence, soft-matter electrostatics, often formulated within the Poisson-Boltzmann (PB) paradigm, needs to be implemented with the self-consistent boundary condition [10], superseding the assumptions of constant charge vs constant potential dichotomy [11]. However, recent work uncovered charge regulation phenomena that cannot be rationalized even within the modified boundary conditions framework [12]. In fact, the interaction of two planar, chargeable surfaces in a bathing electrolyte was shown to be much richer than what could be predicted based on the constant charge vs constant potential phenomenology: the charge symmetry itself can become broken and the interaction turning attractive instead of being, as expected otherwise, repulsive. This also ties in with recent proposals that the attractive non-DLVO (Derjaguin-Landau-Verwey-Overbeek) forces between colloidal surfaces, exhibiting adsorption and dissociation equilibria are unrelated to ion-ion correlations but depend rather directly on the charge regulation mechanisms [13].

Reconstructed lamellae and bilayer systems with fixed charges are well understood both experimentally and theoretically [14–16]. Biological membrane stacks, however, generally have a much more complex electrostatics. We take thylakoid membranes in plants and photosynthetic bacteria as examples. They typically consist of ≈ 10 bilayers, stacked on top of each other to form grana, the light-harvesting organelles. The organization of these lamellae is obviously highly heterogeneous, since they are the carriers of the photosynthetic proteins. Thylakoid stacking has been shown long ago to be driven by electrostatics [17–19], and up to only recently, the classic PB paradigm has been implemented and extended to quantify experiments on thylakoid stacking [20]. However, the charges at the thylakoid membranes are obviously not constant, but depend on the equilibration through two relevant processes: (de)protonation and (de)phosphorylation [21, 22], frequently leading to the observation of asymmetrically charged membranes [21, 22]. Given that the buildup of grana by thylakoids is dynamic and light dependent, and very little is still known about the regulation of this process [23–25], a better understanding of the effect of charge regulation on membrane stacks is generally called for. Physical theory can play a crucial role, as we show by elucidating the effect played by charge regulation in a membrane stack, in which the embedding environment is taken into account.

II. MODEL AND FORMALISM

We consider an array of N charge-regulated, equally-spaced, parallel membranes of negligible thickness [26] immersed in a solvent of permittivity $\varepsilon (= \varepsilon_r \varepsilon_0$ with the relative permittivity ε_r and the permittivity of vacuum ε_0) as depicted in Fig. 1. In a three-dimensional Cartesian coordinate system the first surface is located at $z = 0$ and the N -th surface at $z = L$, implying a separation $\Delta L = L/(N - 1)$ between consecutive surfaces. As it is the case for proteins or membranes, the

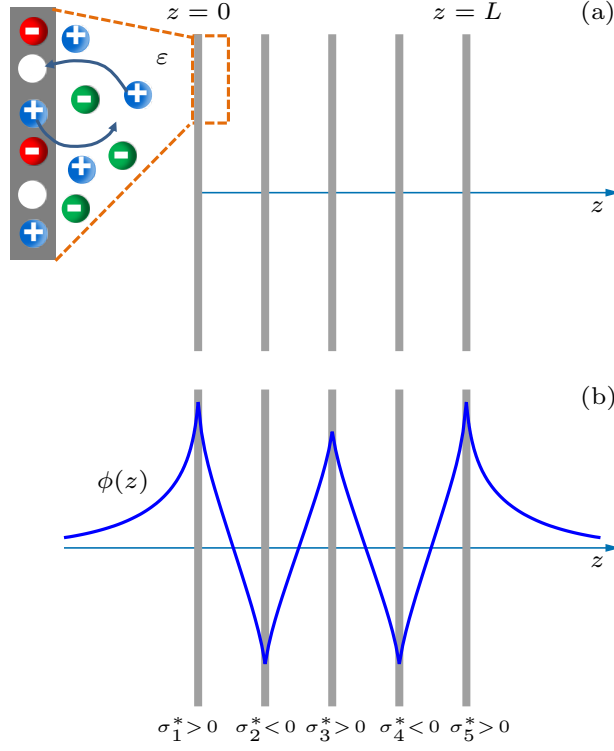


FIG. 1. (a) Sketch of our system consisting of an array of N charge-regulated, equally-spaced, parallel surfaces immersed in a solvent of permittivity ε . The case depicted here corresponds to $N = 5$. The surfaces are placed perpendicularly to the z -axis with the first and the last ones being situated at $z = 0$ and $z = L$, respectively. As shown under magnification, each surface contains fixed negative charges (red circles) and neutral sites (white circles). The surfaces are charge regulated via (de)protonation (blue circles) of these sites. The green circles indicate the mobile anions in the fluid. (b) Under certain circumstances the surfaces can become alternately positively ($\sigma_j^* > 0$) and negatively ($\sigma_j^* < 0$) charged; the corresponding electrostatic potential profile $\phi(z)$ is shown by the blue line.

surfaces consist of fixed negative charges with surface number density M and neutral sites with surface number density $\theta M = 1/a^2$ where (de)protonation can occur. Here we consider the case $\theta = 2$ for which the surface charge density in units of e/a^2 on the j th surface can vary in the interval $\sigma_j^* \in [-\frac{1}{2}, \frac{1}{2}]$ (see [12]).

The grand potential per unit surface area in the units of $k_B T = 1/\beta$ corresponding to our system is then given by [12] (see also [27, 28])

$$\begin{aligned} \beta\Omega[\sigma^*] = & -\frac{\varepsilon}{\beta e^2} \int_{-\infty}^{\infty} dz \left[\kappa^2 (\cosh(\phi(z)) - 1) + \frac{1}{2} (\phi'(z))^2 \right] \\ & + \frac{1}{a^2} \sum_{j=1}^N \left[\sigma_j^* \phi_j - \alpha \eta_j - \frac{\chi \eta_j^2}{2} + \eta_j \ln \eta_j + (1 - \eta_j) \ln(1 - \eta_j) \right], \end{aligned} \quad (1)$$

where ϕ is the dimensionless electrostatic potential satisfying the PB equation $\phi'' = \kappa^2 \sinh \phi$ (see

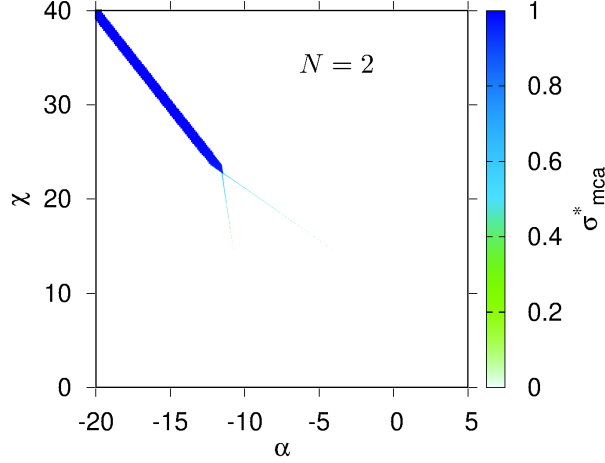


FIG. 2. Variation of the quantity σ_{mca}^* (defined in Eq. (2)) with the parameters α and χ for $N = 2$ charge-regulated interacting surfaces immersed in a solvent. The surfaces are considered to be fixed in space with a dimensionless separation $\kappa\Delta L \approx 1$.

[29]) with the inverse Debye length κ and the Neumann boundary conditions at the surfaces set by $\sigma^* = (\sigma_1^*, \dots, \sigma_N^*)$. The electrostatic potential and the fraction of sites occupied by protons at the j th surface are given by ϕ_j and η_j , respectively, where the latter obeys the relation $\eta_j = \sigma_j^* + 1/2$. The terms containing ϕ in Eq. (1) correspond to the electrostatic field energy and the logarithmic terms are an entropic contribution. As in Ref. [12], the term $-\alpha\eta_j$ describes the non-electrostatic adsorption free energy penalty per ion and the term $-\frac{1}{2}\chi\eta_j^2$ proportional to the Flory-Huggins parameter χ is the change in the nonelectrostatic interaction between adsorbed ions on neighboring sites upon (de)protonation. Nonelectrostatic interaction between adsorbed ions may arise from the formation of complex hydrogen bonded network of water molecules or from forces of quantum-chemical origin such as van der Waals (vdW) and/or chemical bonding interactions, that could be of repulsive as well as attractive nature. The equilibrium values of σ_j^* minimize the grand potential $\beta\Omega[\sigma^*]$ in Eq. (1) (see Appendix for details).

III. RESULTS AND DISCUSSION

The mean charge asymmetry

$$\sigma_{\text{mca}}^* = \frac{1}{N-1} \sum_{j=1}^{N-1} |\sigma_j^* - \sigma_{j+1}^*| \in [0, 1] \quad (2)$$

allows one to distinguish between equally ($\sigma_{\text{mca}}^* = 0$) and unequally ($\sigma_{\text{mca}}^* > 0$) charged neighboring surfaces of the stack. The maximal value $\sigma_{\text{mca}}^* = 1$ corresponds to a configuration with all surfaces being completely charged ($|\sigma_j^*| = \frac{1}{2}$) with alternating positive and negative signs. In the following, we discuss the behavior of σ_{mca}^* for a varying number of surfaces in the stack as well as for varying strengths of the parameters α and χ . Unless stated otherwise, we consider surfaces with $a = 1$ nm immersed in an aqueous electrolyte solution ($\epsilon_r \approx 80$) at $T = 300$ K. Please note that for these values of ϵ_r and T , an ionic strength of 10 mM results in a Debye length $\kappa^{-1} \approx 3$ nm.

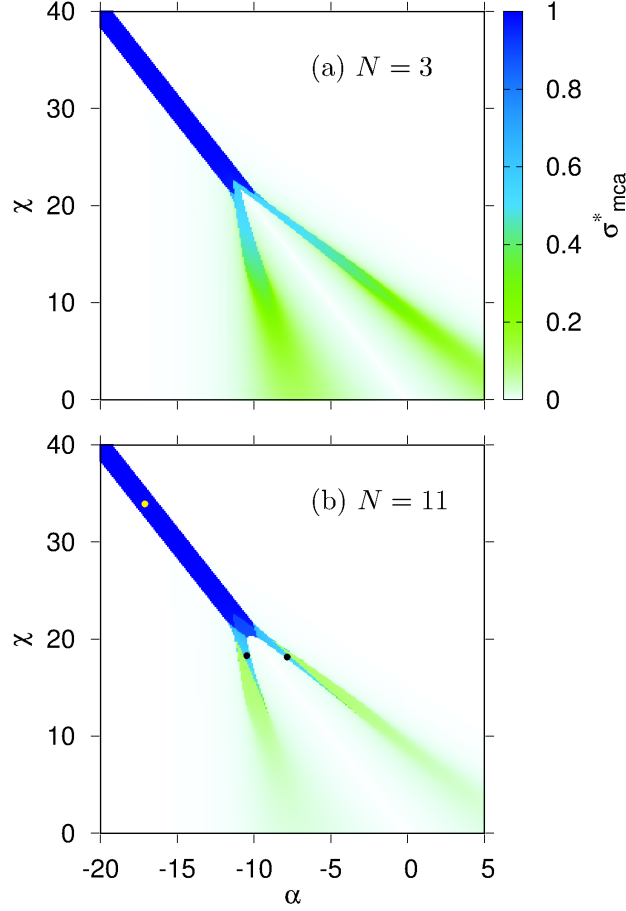


FIG. 3. Variation of the quantity σ_{mca}^* (defined in Eq. (2)) with the interaction parameters α and χ for stacks with (a) $N = 3$ and (b) $N = 11$ charge-regulated interacting surfaces immersed in a solvent. The surfaces in each case are considered to be fixed in space with a dimensionless separation $\kappa\Delta L \approx 1$ between two consecutive surfaces. The yellow (light) and the black bullets in the lower panel represent points considered in Figs. 5 and 6.

First we consider the simplest case of $N = 2$ surfaces, which differs from the situation considered in Ref. [12], where the regions outside the stack were not included. Their presence may influence the charge regulation at the surfaces and in turn affect the charge asymmetry observed in Ref. [12], which results from a tradeoff among the energy costs due to ion-surface, in-plane ion-ion and surface-surface interactions. However, as one can infer from the colored regions in Fig. 2, depending upon the values of the parameters α and χ , the surfaces can still be unequally charged. For $\alpha < \alpha_0 (\approx -11.4)$ a dark blue region appears around the line $\chi = -2\alpha$ with $\sigma_{mca}^* \approx 1$, implying that the surfaces are oppositely charged with $|\sigma_1^*| \approx |\sigma_2^*| \approx \frac{1}{2}$. For $\alpha > \alpha_0$, two very thin tails with lower asymmetry between σ_1^* and σ_2^* appear on either side of the line $\chi = -2\alpha$. Qualitatively, these results are in perfect agreement with Fig. 2(b) of Ref. [12]. The outside regions influence the asymmetric charge regulation only quantitatively, e.g., by giving rise to a thinning of the two tails in Fig. 2 as compared to Fig. 2(b) of Ref. [12].

Now we consider stacks with more than two surfaces. As pairwise electrostatic attractions

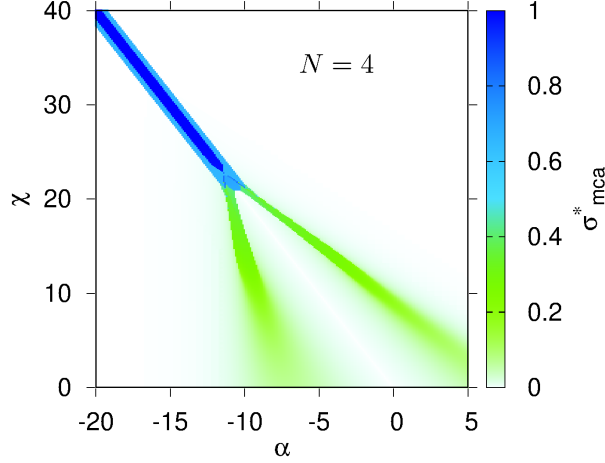


FIG. 4. Variation of the quantity σ_{mca}^* (defined in Eq. (2)) with the interaction parameters α and χ for a stack of $N = 4$ charge-regulated interacting surfaces immersed in a solvent. The surfaces are considered to be fixed in space with a dimensionless separation $\kappa\Delta L \approx 1$ between two consecutive surfaces.

between consecutive surfaces promote a lowering of the grand potential of the system, one would naturally expect the occurrence of alternatingly positively and negatively charged surfaces within the stack, similar to the case of two surfaces. Consequently, the local electrostatic potential would exhibit “oscillations” (see Fig. 1(b) for an example with $N = 5$ surfaces) that would modify the value of the Donnan potential [30], making it effectively vanish. Compared to the case of $N = 2$ in Fig. 2, the colored regions in the α - χ plane are broadened for $N > 2$ (see Figs. 3 and 4).

Figure 3 shows the mean charge asymmetry σ_{mca}^* for odd numbers N of surfaces in the stack. Upon increasing $N \geq 3$, the dark blue region with the highest asymmetry remains almost unaffected but the tails shrink. Inside the dark blue region close to the line $\chi = -2\alpha$, the entropic terms in Eq. (1) almost vanish and the terms involving α and χ nearly cancel each other such that the electrostatic attraction between consecutive surfaces gives rise to the dominant contribution to the grand potential. The key observation is that this electrostatic contribution is invariant upon exchanging all signs of the surface charges. By virtue of a slight preference for filled or empty sites for $\chi \gtrsim -2\alpha$ or $\chi \lesssim -2\alpha$, respectively, one observes crossovers between different charging patterns upon changing χ . For example, for $N = 3$ (see Fig. 3(a)), the charge distribution changes from $(-, +, -)$ with a net negative charge for $\chi < -2\alpha$ to $(+, -, +)$ with a net positive charge for $\chi > -2\alpha$. Here ‘+’ and ‘-’ represent charge densities σ_j^* of approximately $+\frac{1}{2}$ and $-\frac{1}{2}$, respectively. As α is increased beyond the dark blue region, two more regions (tails) with lower charge asymmetry are obtained. For $N = 3$, in the upper (bluish) part of the lower tail (below the line $\chi = -2\alpha$) in Fig. 3(a), the charge distribution is $(0^+, -, 0^+)$, where 0^+ represents a slightly positive charge density. Along the lower tail, the surfaces with charge densities 0^+ become more negatively charged. However, their charge densities differ from the middle surface within the entire greenish region. Exactly the same phenomenon is observed within the upper tail albeit with 0^+ and $-$ being replaced by 0^- and $+$, respectively. Moreover, similar trends are observed for $N = 11$ (see Fig. 3(b)) as well.

Next, we consider the case of even numbers N of surfaces in the stack (see Fig. 4). A significant difference compared to odd N is observed regarding the charge distribution among the surfaces

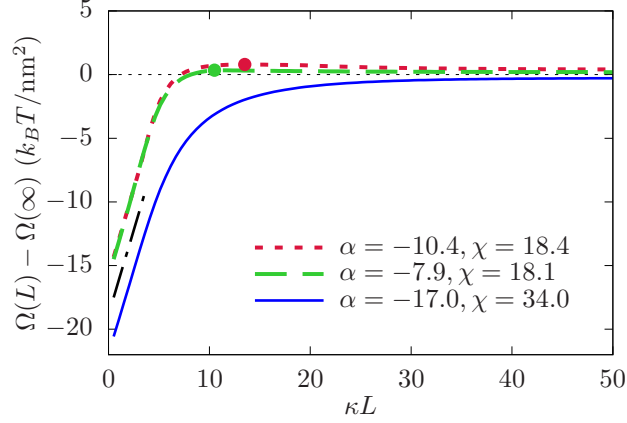


FIG. 5. Binding energy per cross-sectional area of a stack of $N = 11$ surfaces as a function of the dimensionless stack width κL for three different combinations of the interaction parameters α and χ . The blue solid, red dotted, and green dashed lines correspond to points in the dark blue region, the lower tail, and the upper tail of Fig. 3(b), respectively. The binding energy increases within the entire considered range of κL for the blue curve as the electrostatic interaction is strongest there. For the other cases, the electrostatic interaction is weaker such that tiny barriers (marked by the large dots) occur. The dash-dotted straight line depicts a slope of $2.66 k_B T / \text{nm}^2$, which corresponds to the asymptotic disjoining pressure at small stack widths $\kappa L \lesssim 4 \ll N - 1 = 10$ and $\kappa \approx 0.1027 \text{ nm}^{-1}$.

within the dark blue region close to the line $\chi = -2\alpha$. For even N and alternately charged surfaces the total charge of all the surfaces is always zero. Therefore, with increasing χ , a mere flipping of signs of the charges on each surface is not favorable as it does not allow adsorption of more protons onto the surfaces. Consequently, a competition between the electrostatic interaction energy and the contribution of the term involving χ in Eq. (1) takes place which leads to a very different reorganization of charges among the surfaces. For example, within the blue region of Fig. 4, the distribution of charges inside the stack of $N = 4$ surfaces changes from $(-, +, -, -)$ for $\chi < -2\alpha$ via $(-, +, -, +)$ for $\chi \approx -2\alpha$ to $(+, +, -, +)$ for $\chi > -2\alpha$. Although in the configurations $(-, +, -, -)$ and $(+, +, -, +)$ one pair of surfaces repels each other electrostatically, they are favorable due to the ion-ion interaction at each surface. Inside the lower tail in Fig. 4 the charge distribution is of the type $(0^+, -, 0^+, 0^-)$ or $(0^+, -, 0^-, 0^-)$ in the upper part whereas it is of the type $(0^-, -, -, 0^-)$ in the lower part. For the upper tail, one just needs to invert the signs. Exactly the same phenomenon occurs for $N = 10$ (see Fig. A1 in the Appendix). So far we have considered the case $\kappa \Delta L \approx 1$ only. With decreasing separation between the surfaces, the electrostatic pair interaction becomes stronger and the dark blue region spreads to dominate over the tails (see Fig. A1 in the Appendix).

After calculating the equilibrium surface charge densities σ_j^* for fixed parameters α , χ , and N as functions of the stack width L and using Eq. (1), one obtains the grand potential per unit cross-sectional area $\Omega(L)$. In the limit $L \rightarrow \infty$, the electrostatic interaction between the surfaces vanishes. The binding energy of the stack $\Omega(L) - \Omega(\infty)$ is shown in Fig. 5 as a function of the dimensionless stack width κL for $N = 11$ and three different combinations of the parameters α and χ . In all three cases, the binding energy $\Omega(L) - \Omega(\infty)$ increases initially, implying that the disjoining pressure $-\partial\Omega(L)/\partial L$ within the stack is attractive for small widths L . For high mean

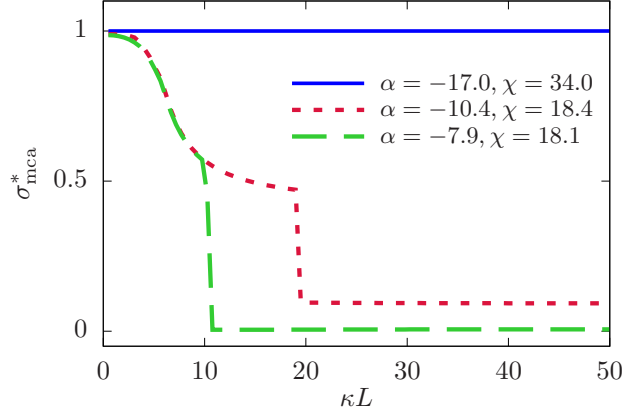


FIG. 6. Mean charge asymmetry σ_{mca}^* for a stack of $N = 11$ surfaces as a function of the dimensionless stack width κL for the three combinations of the interaction parameters α and χ considered in Fig. 5. The blue curve corresponds to a point (marked with bullet) on the $\chi = -2\alpha$ line in Fig. 3(b) where extreme charge asymmetry leading to $\sigma_{\text{mca}}^* \approx 1$ prevails for the entire range of separations shown here. The other two lines correspond to points which, for very short separations, lie within the dark blue region, then fall within the light blue regions of the tails before making a transition to the green or white regions with likely charged surfaces.

charge asymmetry $\sigma_{\text{mca}}^* \approx 1$ and surface separations $\Delta L = L/(N - 1) \ll 1/\kappa$ much smaller than the Debye length $1/\kappa$, no significant screening of the electric field by the ions takes place such that the system can be viewed as a series of $N - 1$ capacitors each charged with approximately half of the maximal surface charge density $|\sigma_j^*|/2 \approx 1/4$. From the electric field energy of such a setup one infers the disjoining pressure $-\partial\Omega(L)/\partial L \simeq -0.273 k_B T/\text{nm}^3 = -11.3 \text{ bar}$ for $L \ll (N - 1)/\kappa$ (see Appendix for details). Note that this value, which corresponds to the slope depicted in Fig. 5 in the range $\kappa L \lesssim 4 \ll N - 1 = 10$, is independent of the number of surfaces N and of the parameters α and χ , as long as high mean charge asymmetry prevails. For the dashed and the dotted curves, which correspond to points within the two tails in Fig. 3(b), the binding energy exhibits a tiny barrier, i.e., the disjoining pressure becomes repulsive for sufficiently thick stacks. The disjoining pressure derived from the solid line, corresponding to parameters α and χ within the dark blue region in Fig. 3(b), is attractive throughout the entire range of κL values shown, as the electrostatic interaction is the strongest here. The corresponding changes in the charge patterns are confirmed by the variation of the mean charge asymmetry σ_{mca}^* shown in Fig. 6. Whereas σ_{mca}^* remains constant at the highest value (≈ 1) throughout the entire range of κL for the blue solid curve, it decreases with increasing κL for the two points in the tails. With increasing separation between the surfaces, the colored regions with asymmetric charge distributions shrink. Consequently, these points first fall within the dark blue region with highest charge asymmetry, then in the sky blue region with lower asymmetry, before making a transition to the green tails indicating unequally but likely charged surfaces or to the white regions with equally charged surfaces.

Finally we discuss the relevance of our results in view of two systems, namely the plant thylakoid membrane and photosynthetic membranes of the family of cyanobacteria, in the same spirit as has been done for the standard PB case, see e.g. [20]. Both systems show stack-like structures

in their light-harvesting organelles. For thylakoids, typically ≈ 10 disks of diameter in the range 300...600 nm are stacked together with interdisk separation $\Delta L \approx 3.5$ nm [20, 23, 24]. The ionic strength of the embedding medium shows two different ranges for monovalent salts [20]: 2...20 mM [22, 31, 32] and 100...200 mM [33]. Up to a salinity of ≈ 10 mM the dimensionless stack width is given by $\kappa L \lesssim 10$, for which the disjoining pressure is attractive for all asymmetrically charged configurations (see Fig. 5). For higher salinities, κL is beyond the barrier of the dashed and the dotted lines in Fig. 5. However, even for the highest salinity of 200 mM with $\kappa L \approx 50$ the disjoining pressure is still attractive within the dark blue region. It has been verified, that the charge-regulation-induced attraction described above dominates quantitatively over the attractive van der Waals force, even for the recently suggested high value of the Hamaker constant $A \approx 4.8 \times 10^{-20}$ J [20], an order of magnitude higher than the standard estimates [34]. Therefore, when asymmetric charging of the stack occurs, the disjoining pressure is dominated by the electrostatic contribution which, at very short separations ($\lesssim 2$ nm), encounters the repulsive hydration force [35]. Similar numbers are found for photosynthetic members of the family of cyanobacteria; typical separation distances lie within 10...120 nm [36, 37] and the concentration of monovalent ions falls in the range of 10...100 mM [38].

IV. CONCLUSIONS

To conclude, we have studied the electrostatic interaction of charge-regulating membranes forming a stack composed of N membranes, embedded in a solution of monovalent salt. Depending on the system parameters, specifically the number of membranes N in the stack, the charge regulation mechanism leads to a complex distribution of attraction and repulsion forces between membranes in the stack. When symmetry broken charge state occurs in the stack, the resulting attraction can easily dominate over the vdW force between the membrane surfaces.

While obtained within a simple model for the charge regulation mechanism, our results have an impact on models of biological membranes, in particular of thylakoid surfaces in grana, the organelles of photosynthesis in plants. The formation of these membrane stacks has been largely discussed in terms of simple electrostatics models based on the standard Poisson-Boltzmann equation for monovalent or divalent salts, in which the charges on the membrane surfaces have been related to the charge state of membrane-embedded protein complexes, notably their phosphorylation status, see, e.g., [20]. Our results confirm the relevance of electrostatics on the stability of membrane stacks; however, they show that a simple balancing of the resulting repulsive forces against attractive vdW forces between two surfaces is generally not sufficient for an understanding of thylakoid stacks. The changes of the charge state on the membranes in the stacks affect the overall charge distribution in a complex manner which may also have a strong influence on the dynamics of thylakoid stack formation, a long-standing open problem in plant science [23, 25], and for photosynthetic cyanobacteria [36]. Changes between the charge load on the membranes, which occur naturally as a function of illumination, are known to affect the packing of the stacks [22]. Hence, the formation of asymmetrically charged membranes is expected to play a major role in the formation of stacks.

APPENDIX

1. The grand potential

Treating the ions as point-like particles and ignoring ion-ion correlation within a mean-field formalism, the grand potential corresponding to our system in units of the thermal energy $\beta = 1/k_B T$ is given by

$$\begin{aligned} \beta\Omega[\eta, \varrho_{\pm}] = & \int_V d^3r \left[\sum_{i=\pm} \varrho_i(\mathbf{r}) \left\{ \ln \left(\frac{\varrho_i(\mathbf{r})}{\zeta_i} \right) - 1 \right\} + \frac{\beta \mathbf{D}(\mathbf{r}, [\varrho_{\pm}, \eta])^2}{2\varepsilon} \right] \\ & + \frac{1}{a^2} \sum_{j=1}^N \left[-\alpha\eta_j - \frac{\chi\eta_j^2}{2} + \eta_j \ln \eta_j + (1 - \eta_j) \ln (1 - \eta_j) \right], \end{aligned} \quad (\text{A1})$$

where the term under the first summation describes the entropic ideal gas contribution formed by the ions with $\varrho_{\pm}(\mathbf{r})$ and ζ_{\pm} denoting the number densities at position $\mathbf{r} \in V$ inside the electrolyte solution and fugacities of the \pm -ions, respectively, and $\eta = (\eta_1, \dots, \eta_N)$ denotes the fraction of sites occupied by protons on each surface. The remaining term under the integral describes the Coulomb interaction among all charges in the system in a mean-field-like fashion in terms of the electric displacement field \mathbf{D} . The remaining quantities have the same meaning as defined in the main text.

Minimization of the grand potential in Eq. (A1) with respect to the ionic density profiles ϱ_{\pm} provides the Euler-Lagrange equation which ultimately leads to the PB equation $\phi'' = \kappa^2 \sinh(\phi)$ subjected to Neumann boundary conditions at the surfaces set by the prescribed ion adsorption profile η . Here ϕ is the dimensionless electrostatic potential expressed in units of βe . Hence the equilibrium ion density profiles $\varrho_{\pm}[\eta]$ and the equilibrium electrostatic potential $\phi[\eta]$ are functionals of the adsorption profile η . Inserting $\varrho_{\pm}[\eta]$ in Eq. (A1) one obtains the grand potential merely in terms of the adsorption profile η :

$$\begin{aligned} \beta\Omega[\sigma^*] = & -\frac{\varepsilon}{\beta e^2} \int_{-\infty}^{\infty} dz \left[\kappa^2 (\cosh(\phi(z)) - 1) + \frac{1}{2} (\phi'(z))^2 \right] \\ & + \frac{1}{a^2} \sum_{j=1}^N \left[\sigma_j^* \phi_j - \alpha\eta_j - \frac{\chi\eta_j^2}{2} + \eta_j \ln \eta_j + (1 - \eta_j) \ln (1 - \eta_j) \right], \end{aligned} \quad (\text{A2})$$

where $\kappa^{-1} = \sqrt{\varepsilon/(2\beta e^2 I)}$ is the Debye length with I being the ionic strength. This is the expression for the grand potential we provide in the main text.

2. Minimization of the grand potential

The integral in the first line of Eq. (A2) can be decomposed in the following way:

$$\begin{aligned}
\beta\Omega[\sigma^*] = & -\frac{\varepsilon}{\beta e^2} \int_{-\infty}^0 dz \left[\kappa^2 (\cosh(\phi(z)) - 1) + \frac{1}{2} (\phi'(z))^2 \right] \\
& -\frac{\varepsilon}{\beta e^2} \int_0^L dz \left[\kappa^2 (\cosh(\phi(z)) - 1) + \frac{1}{2} (\phi'(z))^2 \right] \\
& -\frac{\varepsilon}{\beta e^2} \int_L^\infty dz \left[\kappa^2 (\cosh(\phi(z)) - 1) + \frac{1}{2} (\phi'(z))^2 \right] \\
& + \frac{1}{a^2} \sum_{j=1}^N \left[\sigma_j^* \phi_j - \alpha \eta_j - \frac{\chi \eta_j^2}{2} + \eta_j \ln \eta_j + (1 - \eta_j) \ln (1 - \eta_j) \right].
\end{aligned} \tag{A3}$$

First, we consider the first integral (from $-\infty$ to 0) in Eq. (A3). One can rewrite it as

$$\begin{aligned}
I_1 = & -\frac{\varepsilon}{\beta e^2} \int_{-\infty}^0 dz \left[\kappa^2 (\cosh(\phi(z)) - 1) + \frac{1}{2} (\phi'(z))^2 \right] \\
= & -\int_{-\infty}^0 dz \left[2I (\cosh(\phi(z)) - 1) + \frac{\varepsilon}{2\beta e^2} (\phi'(z))^2 \right].
\end{aligned} \tag{A4}$$

Multiplying both sides of the PB equation by ϕ' one obtains

$$\phi' \phi'' = \kappa^2 \sinh(\phi) \phi', \tag{A5}$$

which can be rewritten as

$$\frac{1}{2} ((\phi')^2)' = \kappa^2 (\cosh(\phi))'. \tag{A6}$$

Integrating Eq. (A6) with respect to z and using $\phi(-\infty) = \phi'(-\infty) = 0$ gives

$$\frac{1}{2} (\phi')^2 = \kappa^2 (\cosh(\phi) - 1), \tag{A7}$$

which leads to

$$2I (\cosh(\phi) - 1) = \frac{\varepsilon}{2\beta e^2} (\phi')^2. \tag{A8}$$

Using Eq. (A8), Eq. (A4) simplifies to

$$I_1 = -\int_{-\infty}^0 dz \frac{\varepsilon}{\beta e^2} (\phi'(z))^2. \tag{A9}$$

If we consider only the semi-infinite geometry from $-\infty$ to 0 having a charged surface at $z = 0$, the PB equation for this setup is analytically solvable and its solution is well known [29, 39]:

$$\phi(z) = 4 \operatorname{artanh}(\gamma \exp(\kappa z)); \quad \gamma = \tanh\left(\frac{\phi(0)}{4}\right). \quad (\text{A10})$$

Taking the derivative with respect to z , one obtains

$$\phi'(z) = 4\kappa\gamma \frac{\exp(\kappa z)}{1 - \gamma^2 \exp(2\kappa z)}. \quad (\text{A11})$$

Therefore,

$$\begin{aligned} \int_{-\infty}^0 dz (\phi'(z))^2 &= 16\kappa^2\gamma^2 \int_{-\infty}^0 dz \frac{\exp(2\kappa z)}{(1 - \gamma^2 \exp(2\kappa z))^2} \\ &= 8\kappa \int_{-\infty}^0 dz \frac{2\kappa\gamma^2 \exp(2\kappa z)}{(1 - \gamma^2 \exp(2\kappa z))^2} \\ &= 8\kappa \int_{-\infty}^0 dz \left(\frac{d}{dz} \frac{1}{1 - \gamma^2 \exp(2\kappa z)} \right) \\ &= 8\kappa \left[\frac{1}{1 - \gamma^2 \exp(2\kappa z)} \right]_{z=-\infty}^0 \\ &= 8\kappa \left(\frac{1}{1 - \gamma^2} - 1 \right) \\ &= \frac{8\kappa\gamma^2}{1 - \gamma^2}. \end{aligned} \quad (\text{A12})$$

Using this, Eq. (A9) becomes

$$\begin{aligned} I_1 &= -\frac{\varepsilon}{\beta e^2} \frac{8\kappa\gamma^2}{1 - \gamma^2} \\ &= -\frac{8\kappa\varepsilon}{\beta e^2} \frac{\tanh\left(\frac{\phi(0)}{4}\right)^2}{1 - \tanh\left(\frac{\phi(0)}{4}\right)^2} \\ &= -\frac{8\kappa\varepsilon}{\beta e^2} \sinh\left(\frac{\phi(0)}{4}\right)^2. \end{aligned} \quad (\text{A13})$$

Similarly, it can be shown that the integral from L to ∞ in Eq. (A3) boils down to

$$I_2 = -\frac{8\kappa\varepsilon}{\beta e^2} \sinh\left(\frac{\phi(L)}{4}\right)^2. \quad (\text{A14})$$

Using Eqs. (A13) and (A14), in Eq. (A3), one arrives at the expression

$$\begin{aligned} \beta\Omega[\sigma^*] = & -\frac{8\kappa\epsilon}{\beta e^2} \left[\sinh\left(\frac{\phi(0)}{4}\right)^2 + \sinh\left(\frac{\phi(L)}{4}\right)^2 \right] \\ & -\frac{\epsilon}{\beta e^2} \int_0^L dz \left[\kappa^2 (\cosh(\phi(z)) - 1) + \frac{1}{2} (\phi'(z))^2 \right] \\ & + \frac{1}{a^2} \sum_{j=1}^N \left[\sigma_j^* \phi_j - \alpha \eta_j - \frac{\chi \eta_j^2}{2} + \eta_j \ln \eta_j + (1 - \eta_j) \ln(1 - \eta_j) \right]. \end{aligned} \quad (\text{A15})$$

This is the expression we minimize to obtain the equilibrium profiles for $\sigma^* = (\sigma_1^*, \dots, \sigma_N^*)$. The minimization is done by two nested loops: the inner one calculates $\phi(z)$ for fixed σ^* profiles and the outer one performs a steepest descent step to minimize Ω . The iteration is done until convergence is reached.

3. Variation of the stack width

In the main text, we have shown results for the case of separation $\kappa\Delta L \approx 1$ between two consecutive surfaces in the stack. When this separation changes, the electrostatic interaction between the surfaces, which is at the origin of the observed charge asymmetry [12], also changes. As a result, for given α and χ , the charge distribution inside the stack changes with varying $\kappa\Delta L$. This can be inferred from Fig. A1 where we have shown the quantity σ_{mca}^* for two different $\kappa\Delta L$ values. With decreasing separation between the surfaces, their electrostatic attraction becomes stronger and it dominates over other interactions present in the system for a wider range of α and χ parameters. Of course, the opposite happens when increasing the inter-surface separation: the electrostatic interaction becomes weaker and the colored region of asymmetric charge distributions becomes narrower.

As discussed in the main text, for an even number of surfaces inside the stack, a reorganization of the charge distribution takes place across the line $\chi = -2\alpha$ and consequently, σ_{mca}^* changes color (see Fig. 4 of the main text). With increasing number N of surfaces inside the stack, this feature remains as it has nothing to do with total number of surfaces inside the stack as long as N is even. However, the contrast in σ_{mca}^* values becomes lower as the denominator in Eq. (2) of the main text increases with increasing N . As a result, the color contrast within the blue region in the left panel of Fig. A1 is lower compared to that in Fig. 4 of the main text.

4. Disjoining pressure in the small stack width limit

As mentioned in the main text, all the three curves in Fig. 5 increase linearly for very short stack widths $\kappa L \lesssim 4$. At such short separations, electrostatics is almost unscreened and each oppositely and highly charged pair of surfaces (with charge densities $|\sigma| \approx 0.5 e/\text{nm}^2$) inside the stack acts like a capacitor. So the total energy of the system is, besides the contribution of the outer parts, a sum of these capacitor energies. Each surface contributes to its both sides; therefore, half of their charges contribute to each capacitor. As a result, the L -dependent part of the grand potential per

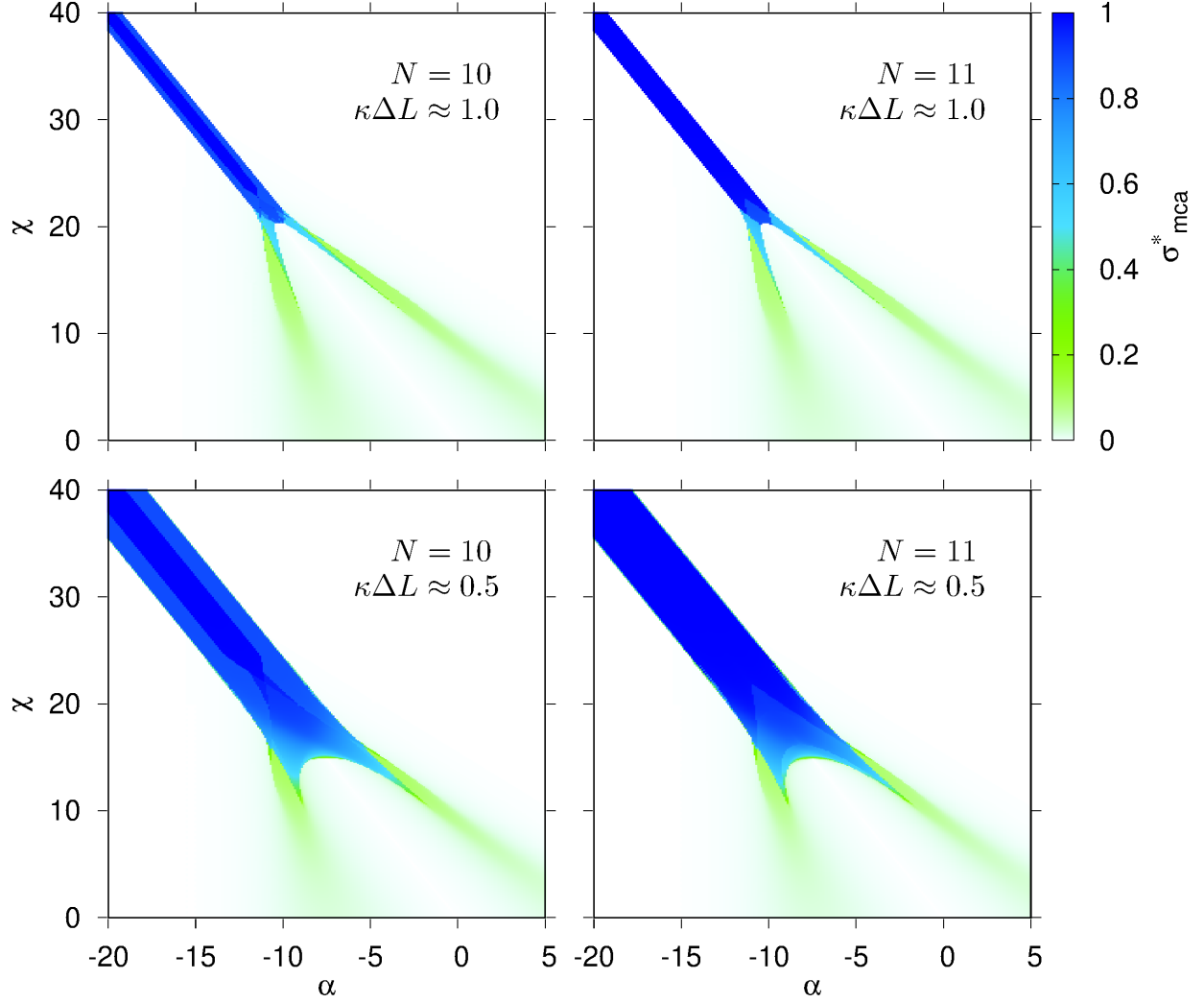


FIG. A1. Variation of the quantity σ_{mca}^* for stacks of $N = 10$ (left panel) and $N = 11$ (right panel) charge-regulated interacting surfaces with the interaction parameters α and χ and with varying dimensionless separation $\kappa\Delta L$ between two consecutive surfaces. As one can see, with decreasing $\kappa\Delta L$ the dark blue region with the highest charge-asymmetry spreads.

unit cross-sectional area equals

$$\Omega = \frac{\sigma^2 \Delta L (N-1)}{8\epsilon_0 \epsilon_r} = \frac{\sigma^2 L}{8\epsilon_0 \epsilon_r} \quad (\text{A16})$$

The factor of ‘8’ in the denominator results from the fact that half of the total charge on each surface contributes to a capacitor. The corresponding disjoining pressure $-\frac{\partial(\Omega)}{\partial(L)}$ then equals to $-\frac{\sigma^2}{8\epsilon_0 \epsilon_r} = -0.273 k_B T / \text{nm}^3$, which, when divided by $\kappa \approx 0.1027 \text{ nm}^{-1}$, matches perfectly with the

observed slope ($2.66 k_B T / \text{nm}^2$) of the linear parts of the curves in Fig. 5.

-
- [1] K. Linderstrøm-Lang, C. R. Trav. Lab. Carlsberg **15**, 1 (1924).
 - [2] J. Kirkwood and J. B. Shumaker, Proc. Natl. Acad. Sci. USA **38**, 855 (1952).
 - [3] R. A. Marcus, J. Chem. Phys. **23**, 1057 (1955).
 - [4] S. Lifson, J. Chem. Phys. **26**, 727 (1957).
 - [5] M. Lund and B. Jönsson, Quart. Rev. Biophys. **46**, 265 (2013).
 - [6] N. Adžić and R. Podgornik, Phys. Rev. E **91**, 022715 (2015).
 - [7] R. Podgornik, J. Chem. Phys. **149**, 104701 (2018).
 - [8] Y. Avni, T. Markovich, R. Podgornik, and D. Andelman, Soft Matter **14**, 6058 (2018).
 - [9] A. P. dos Santos and Y. Levin, Phys. Rev. Lett. **122**, 248005 (2019).
 - [10] B. W. Ninham and V. A. Parsegian, J. Theor. Biol. **31**, 405 (1971).
 - [11] T. Markovich, D. Andelman, and R. Podgornik, Europhys. Lett. **113**, 26004 (2016).
 - [12] A. Majee, M. Bier, and R. Podgornik, Soft Matter **14**, 985 (2018).
 - [13] A. M. Smith, P. Maroni, and M. Borkovec, Phys. Chem. Chem. Phys. **20**, 158 (2018).
 - [14] T. Markovich, D. Andelman, and R. Podgornik, in *Handbook of Lipid Membranes*, Ed. by C. Safinya and J. Rädler (Taylor & Francis, 2019).
 - [15] L. Herrmann, A. Johner, and P. Kékicheff, Phys. Rev. Lett. **113**, 268302 (2014).
 - [16] M. Hishida, Y. Nomura, R. Akiyama, Y. Yamamura, and K. Saito, Phys. Rev. E **96**, 040601(R) (2017).
 - [17] J. Barber, FEBS Lett. **118**, 1 (1980).
 - [18] B. T. Rubin and J. Barber, Biochim. Biophys. Acta **592**, 87 (1980).
 - [19] J. Barber, Ann. Rev. Plant Physiol. **33**, 261 (1982).
 - [20] S. Puthiyaveetil, B. van Oort, and H. Kirchhoff, Nat. Plants **3**, 17020 (2017).
 - [21] J. F. Allen, Biochim. Biophys. Acta **1098**, 275 (1992).
 - [22] R. Kaňa and Govindjee, Front. Plant Sci. **7**, 1849 (2016).
 - [23] L. Mustárdy, K. Buttle, G. Steinbach, and G. Garab, Plant Cell **20**, 2552 (2008).
 - [24] H. Kirchhoff, C. Hall, M. Wood, M. Herbstová, O. Tsabari, R. Nevo, D. Charuvi, E. Shimoni, and Z. Reich, Proc. Natl. Acad. Sci. USA **108**, 20248 (2011).
 - [25] H. Kirchhoff, Plant Sci. **266**, 76 (2018).
 - [26] The underpinnings and limitations of this approximation are discussed in Ref. [14].
 - [27] D. Harries, R. Podgornik, V. A. Parsegian, E. Mar-Or, and D. Andelman, J. Chem. Phys. **124**, 224702 (2006).
 - [28] M. Tagliazucchi, M. O. de la Cruz, and I. Szleifer, Proc. Natl. Acad. Sci. USA **107**, 5300 (2010).
 - [29] W. B. Russell, D. A. Saville, and W. R. Schowalter, *Colloidal Dispersions* (Cambridge University Press, Cambridge, 1989).
 - [30] P. J. Bassar and A. J. Grodzinsky, Biophys. Chem. **46**, 57 (1993).
 - [31] M. J. Sculley, J. T. Duniec, S. W. Thorne, W. S. Chow, and N. K. Boardman, Arch. Biochem. Biophys. **201**, 339 (1980).
 - [32] J. A. Cruz, C. A. Sacksteder, A. Kanazawa, and D. M. Kramer, Biochem. **40**, 1226 (2001).
 - [33] K. Philippar and J. Soll, *Intracellular transport: solute transport in chloroplast, mitochondria, peroxi-*

- somes and vacuoles, and between organelles. In: Plant Solute Transport*, Ed. by A. R. Yeo and T. J. Flowers (Blackwell Publishing, pp. 133-193, 2007).
- [34] R. Podgornik, R. H. French, and V. A. Parsegian, *J. Chem. Phys.* **124**, 044709 (2006).
 - [35] J. Barber, *Biochim. Biophys. Acta* **594**, 253 (1980).
 - [36] L.-R. Stingaciu, H. O'Neill, M. Liberton, V. S. Urban, H. B. Pakrasi, and M. Ohl, *Sci. Rep.* **6**, 19627 (2016).
 - [37] A. M. L. van de Meene, W. P. Sharp, J. H. McDaniel, H. Friedrich, W. F. J. Vermaas, and R. W. Roberson, *Biochim. Biophys. Acta* **1818**, 1427 (2012).
 - [38] F. J. van Eerden, D. H. de Jong, A. H. de Vries, T. A. Wassenaar, and S. J. Marrink, *Biochim. Biophys. Acta* **1848**, 1319 (2015).
 - [39] R. J. Hunter, *Foundations of colloid science* (Clarendon Press, Oxford, 1989).